International Journal of
Molecular Sciences

MDPI

Article

Experimental and Computational Studies on Structure and Energetic Properties of Halogen Derivatives of 2-Deoxy-D-Glucose

Marcin Ziemniak [1,*], Anna Zawadzka-Kazimierczuk [1], Sylwia Pawlędzio [1], Maura Malinska [1], Maja Sołtyka [2], Damian Trzybiński [1], Wiktor Koźmiński [1], Stanisław Skora [3], Rafał Zieliński [3], Izabela Fokt [3], Waldemar Priebe [3,*], Krzysztof Woźniak [1] and Beata Pająk [2,*]

[1] Biological and Chemical Research Centre, Department of Chemistry, University of Warsaw, Zwirki i Wigury 101, 02-089 Warszawa, Poland; anzaw@chem.uw.edu.pl (A.Z.-K.); spawledzio@chem.uw.edu.pl (S.P.); mmalinska@chem.uw.edu.pl (M.M.); dtrzybinski@cnbc.uw.edu.pl (D.T.); kozmin@chem.uw.edu.pl (W.K.); kwozniak@chem.uw.edu.pl (K.W.)
[2] Independent Laboratory of Genetics and Molecular Biology, Kaczkowski Military Institute of Hygiene and Epidemiology, Kozielska 4, 01-163 Warsaw, Poland; maja.soltyka@gmail.com
[3] Department of Experimental Therapeutics, The University of Texas MD Anderson Cancer Center, 1901 East Rd., Houston, TX 77054, USA; sskora@mdanderson.org (S.S.); RJZielinski@mdanderson.org (R.Z.); ifokt@mdanderson.org (I.F.)
* Correspondence: mziemniak@chem.uw.edu.pl (M.Z.); wpriebe@mac.com (W.P.); bepaj@wp.pl (B.P.)

Citation: Ziemniak, M.; Zawadzka-Kazimierczuk, A.; Pawlędzio, S.; Malinska, M.; Sołtyka, M.; Trzybiński, D.; Koźmiński, W.; Skora, S.; Zieliński, R.; Fokt, I.; et al. Experimental and Computational Studies on Structure and Energetic Properties of Halogen Derivatives of 2-Deoxy-D-Glucose. *Int. J. Mol. Sci.* **2021**, *22*, 3720. https://doi.org/10.3390/ijms22073720

Academic Editor: Daniela Montesarchio

Received: 2 March 2021
Accepted: 31 March 2021
Published: 2 April 2021

Abstract: The results of structural studies on a series of halogen-substituted derivatives of 2-deoxy-D-glucose (2-DG) are reported. 2-DG is an inhibitor of glycolysis, a metabolic pathway crucial for cancer cell proliferation and viral replication in host cells, and interferes with D-glucose and D-mannose metabolism. Thus, 2-DG and its derivatives are considered as potential anticancer and antiviral drugs. X-ray crystallography shows that a halogen atom present at the C2 position in the pyranose ring does not significantly affect its conformation. However, it has a noticeable effect on the crystal structure. Fluorine derivatives exist as a dense 3D framework isostructural with the parent compound, while Cl- and I-derivatives form layered structures. Analysis of the Hirshfeld surface shows formation of hydrogen bonds involving the halogen, yet no indication for the existence of halogen bonds. Density functional theory (DFT) periodic calculations of cohesive and interaction energies (at the B3LYP level of theory) have supported these findings. NMR studies in the solution show that most of the compounds do not display significant differences in their anomeric equilibria, and that pyranose ring puckering is similar to the crystalline state. For 2-deoxy-2-fluoro-D-glucose (2-FG), electrostatic interaction energies between the ligand and protein for several existing structures of pyranose 2-oxidase were also computed. These interactions mostly involve acidic residues of the protein; single amino-acid substitutions have only a minor impact on binding. These studies provide a better understanding of the structural chemistry of halogen-substituted carbohydrates as well as their intermolecular interactions with proteins determining their distinct biological activity.

Keywords: 2-deoxy-D-glucose; 2-DG analogues; hydrogen bonds; energy frameworks; Hirshfeld surface; NMR spectroscopy; The University at Buffalo Pseudoatom Databank (UBDB); glycolysis inhibitors; electrostatic interactions; ligand binding

1. Introduction

2-Deoxy-D-glucose (2-DG) is a synthetic analogue of D-glucose in which a hydroxyl group at C-2 is replaced by a hydrogen atom. Since D-glucose and D-mannose are C-2 epimers and in consequence their deoxygenation at C-2 would produce the same compound, the 2-DG should also be considered an analogue of D-mannose [1] (Figure 1). A significant number of halogen-substituted carbohydrates have been synthesized. Some

of them, the fluorine derivatives, were extensively tested, and 2-deoxy-2-fluoro[^{18}F]-D-glucose has been used in medicine as an imaging agent for positron emission tomography (PET) [2,3]. Other halogen derivatives have been initially considered as potentially useful intermediates in synthetic carbohydrate chemistry [4], and only later considered and tested as potential biologically active agents [5,6]. A significant scientific effort has recently been allocated to develop new drugs targeting cancer metabolism, particularly glucose metabolism, which differs from glucose processing in normal cells [7,8]. 2-DG is considered a promising anticancer drug targeting glucose metabolism of cancer cells [5,9], including melanoma [10], osteosarcoma [11], and others. Its proposed mechanism of action relies on the inhibition of some key enzymes involved in glucose and mannose metabolism. One of those enzymes is hexokinase (HK), responsible for glucose phosphorylation in the first step of glycolysis. HK inhibition leads to significant impairment of glucose metabolism. The other route to disrupt the homeostasis of cancer cells by 2-DG relies on alteration of protein glycosylation and disruption of signaling pathways [9]. Previous studies demonstrated potential antiviral properties of 2-DG [12,13]. More recent computational studies suggested that 2-DG and its derivatives can block viral proteases, which render the virus unable to bind to its receptor [14]. In summary, so far in addition to 2-DG, only 2-deoxy-2-fluoro-D-glucose (2-FG) has been recognized as a potential anticancer compound in cancer therapy [15,16]. Other halogen derivatives of 2-DG were not extensively investigated. Studies comparing different halogen analogues directly with 2-DG have been initiated by us [6] and these studies and our more recent preliminary data (not published) suggest that other 2-DG derivatives should also be considered as potentially useful agents in the treatment or diagnoses of metabolically dependent diseases.

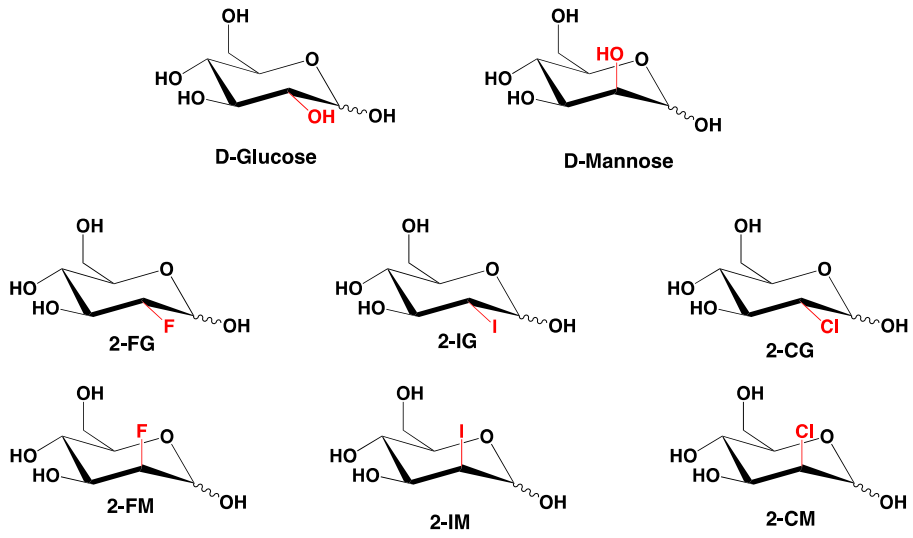

Figure 1. Chemical structures of investigated compounds. These compounds can be considered as 2-substituted D-glucose (Glc) or D-mannose (Man) derivatives.

Despite the potential medical significance of 2-DG derivatives, only a few crystal structures of high quality are available in crystallographic databases (including the parent compound) [17]. This possibly is due to significant difficulties in the preparation of high-quality crystals. Most carbohydrates tend to form amorphic solids, often containing residual solvent. Most of the existing structures are polyfluorinated pyranoses, which are easier to crystallise due to a reduced number of hydroxyl groups [18–20]. There is one structure of 2-FG deposited in the CSD database (deposition number 1296336); however, it has only moderate quality. To our best knowledge, no comprehensive structural study investigating the effects of substitution by different halogens at a given position in the pyranose ring has been conducted. A better understanding of the structural features of this class of carbohydrates, both in the solid state and solution, is necessary to achieve

an in-depth knowledge of their biological and pharmacological properties. It should be noted that there have been several experimental preclinical and clinical studies with 2-DG (and its derivatives), mainly administrated orally. Thus, the existence of their potential polymorphs may have profound medical implications because different crystal forms usually are characterized by different bioavailability [21,22].

High-resolution structural research combined with theoretical calculations provides a better understanding of intra- and intermolecular interactions in the solid state as well as principal energetic features of the structure, including the interaction anisotropy [23] and charge-density distribution [24]. Such findings may relate to biological and pharmacological properties of drug-like molecules and potential drug candidates [25] as well as crystal engineering [26,27]. The structural scaffolding of both 2-DG and its halogen derivatives is composed of moieties capable of forming a complicated set of hydrogen interactions between hydroxyl groups in the pyranose ring. Moreover, the halogen substitution, particularly by bromine and iodine, creates a possibility for halogen-mediated interactions, which is interesting from the structural perspective because studies on halogen bonding in carbohydrates have been limited due to the lack of available crystal structures. Another interesting possibility is to investigate H-bonding with the fluorine atom in a polyhydroxylated system, which is still a matter of debate in structural chemistry [28].

In this paper, the crystal structures of a series of halogenated 2-DG derivatives (Figure 1), namely, 2-deoxy-2-fluoro-D-glucopyranose (2-FG), 2-deoxy-2-fluoro-D-mannopyranose (2-FM), 2-deoxy-2-chloro-D-glucopyranose (2-CG), 2-deoxy-2-chloro-D-mannopyranose (2-CM), and 2-deoxy-2-iodo-D-glucopyranose (2-IG) have been solved and refined by applying single-crystal X-ray diffraction. We described their crystal properties, focusing on analysis of the H-bond network in the supramolecular landscape. Furthermore, the collected data were used in theoretical calculations to reveal more details concerning their crystal packing as well as intra- and intermolecular interactions. Due to the problems with optimizing the conditions and obtaining the appropriate crystals, 2-deoxy-2-iodo-D-mannopyranose (2-IM), 2-deoxy-2-bromo-D-glucopyranose (2-BG), and 2-deoxy-2-bromo-D-mannopyranose (2-BM) have not been analysed so far. Thus, 2-IM and bromo-derivatives are still under scrutiny in our lab, and the results will be published in a separate paper.

Firstly, we performed Hirshfeld surface analysis to obtain a quantitative and qualitative description of interatomic contacts in the structure. Secondly, we calculated some energetic features of the structure, i.e., the total lattice energy and energy frameworks. Next, high-resolution NMR spectral data shed more light on their structural properties in aqueous solution, including anomeric and conformational equilibria. Finally, we use Hirshfeld analysis and computational methods to investigate the binding of 2-FG in several protein structures quantitatively.

As far as we know, this is the first report describing the structure and energetic properties of halogen derivatives of 2-DG.

2. Results and Discussion

2.1. Crystallization and Crystal Morphology

Initial attempts to crystallize 2-DG derivatives from water solution resulted only in a syrup-like amorphous phase, thus only crystallization from organic solvents allowed us to obtain a mixture of crystalline and amorphic, vitreous phases. For each compound, the crystalline phase was composed of aggregates in which monomeric single crystals were observed. The crystals displayed an acicular or columnar habit, and most of them were macroscopically twinned.

2.2. X-ray Diffraction Studies

Single-crystal X-ray diffraction analysis confirmed the identity of all investigated compounds. Most of them crystallize in the orthorhombic $P2_12_12_1$ space group. The only exception is 2-CM, which was forming crystals in the monoclinic $P2_1$ space group. In all cases, the crystal lattice's asymmetric unit contained one molecule of compound (Figure 2).

The 2-CM turned out to be a solvate. The independent part of its unit cell also included one molecule of water (Figure 2). Details of the crystallographic data and refinement parameters are summarized in Table S1 (ESI). Other parameters such as bond lengths, valence, and torsion angle values can be found in the Electronic Supporting Information (Tables S2–S16).

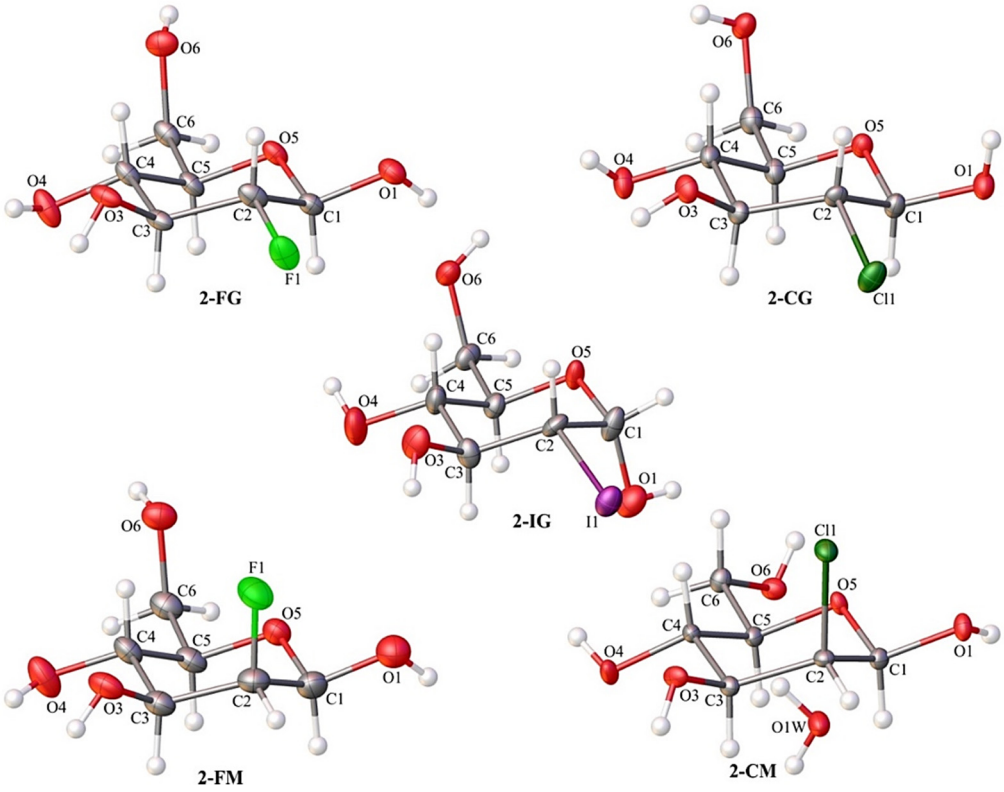

Figure 2. The content of the asymmetric unit of the crystal structures of investigated compounds with the atom numbering scheme. Atomic displacement ellipsoids are shown with 50% probability and the H-atoms are shown as small spheres of arbitrary radius.

2.3. Conformational Analysis of the Pyranose Ring

A common way to describe a monocyclic ring's conformation is to use Cremer-Pople parameters (CP), generalized ring-puckering coordinates in a spherical coordinate system. CP parameters allow for the quantitative and precise definition of puckering conformations [29]. In each structure, the carbohydrate molecule forms a pyranose ring existing in the chair $^4C_1$ (D1) enantiomeric conformer. Calculated CP parameters indicated only minor deviations from the ideal chair geometry ($\theta = 0°$), and the largest deviation is observed for 2-CG ($\theta = 7.8°$). In all investigated compounds, the geometry of pyranose was also highly similar to the parent compound ($\theta = 6.0°$ for the α anomer), indicating that halogen substitution does not alter the ring conformation in any significant way. The other CP parameters are summarized in Table S17. The structural similarity of the pyranose rings in 2-DG derivatives was also visualized by structural alignments (Figure 3).

All these compounds crystallise exclusively as β-anomers, and the only exception is 2-IG, which forms the α-anomer in the crystal state. The C6 hydroxyl group's orientation is axial in most of the studied compounds except 2-CM, where the C6 hydroxyl group is oriented equatorially. In the crystal, the critical factors driving the conformation of the pyranose ring, as well as the orientation of its substituents, are hydrogen bonds. These non-covalent interactions may stabilize a conformation that is not energetically preferred in an aqueous solution, where the prevalence of a given enantiomeric conformer is determined mostly by the orientation of the largest substituent in the pyranose ring. It is

also assumed that both intra- and intermolecular H-bonds between sugar moieties play only a marginal role.

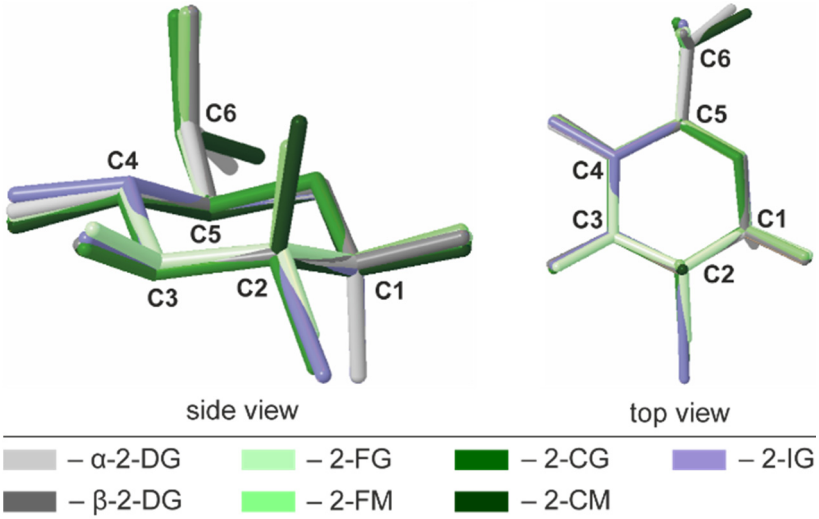

Figure 3. Superimposed structures of investigated halogen derivatives compared to α- and β-anomers of their parent compound.

2.4. Intermolecular Interactions

The substitution of the pyranose C2-atom by halogen atoms of various sizes has a noticeable impact on the supramolecular landscape. The significance of changes concerning the mutual arrangement of molecules and the scheme of intermolecular interactions occurring in their crystals is different for individual compounds. However, some general trends can be noticed. In the case of both fluoro derivatives (2-FG and 2-FM), the changes are relatively subtle. A closer look (Figure 4) reveals β-2-FG and β-2-FM molecules are organized in their crystals almost identically to the β-anomer of 2-DG (β-2-DG) [30]. Moreover, all three compounds display nearly the same unit cell parameters. This isostructurality results from the relatively small size of the fluorine atom, which is often regarded, when connected to carbon, as an isostere of hydrogen. The existence of such a phenomenon also has been reported for other fluorinated organic systems [31,32]. Differences between the crystal structures of β-2-DG, β-2-FG, and β-2-FM become more apparent after a detailed examination of each structure's existing scheme of interactions. Sugar molecules are assembled in complex 3D-frameworks, in which a dense network of hydrogen bonds is present.

In the crystal of the parent compound, the adjacent molecules are held together by O−H···O hydrogen bond (d(D···A) = 2.655(2)–2.808(2) Å; <(D−H···A) = 150–172°; Table S18 (ESI)) interactions, and the crystal network is stabilized by the weak intermolecular C−H···O contacts (d(D···A) = 3.380(2)–3.518(2) Å; <(D−H···A) = 146−147°; Table S18). The fluorine substitution in C2 position results in the intermolecular C−H···F (2-FG) (d(D···A) = 3.325(4) Å; <(D−H···A) = 142°; Table S19) and O−H···F (2-FM) (d(D···A) = 3.002(4) Å; <(D−H···A) = 142(5)°; Table S22) interactions, which replace one of the C−H···O contacts observed in the crystal network of β-2-DG. Different types of interactions involving halogens in 2-FG and 2-FM stem from different positions of the halogen itself (axial in 2-FM and equatorial in 2-FG). Nevertheless, the overall pattern of the intermolecular O−H···O hydrogen bonds is preserved in all compounds mentioned above, and they differ only by the subtle changes of their geometry. The distances between the donor and acceptor of the H-atoms in hydrogen bonds ranged from 2.622(3) to 2.786(3) Å, and from 2.665(4) to 2.846(5) Å for β-2-FG and β-2-FM, respectively. Additionally, their <(D−H···A) angles were in the ranges of 149(4)-175(4)° and 163(5)–171(6)° for β-2-FG and β-2-FM, respectively (Tables S19 and S22).

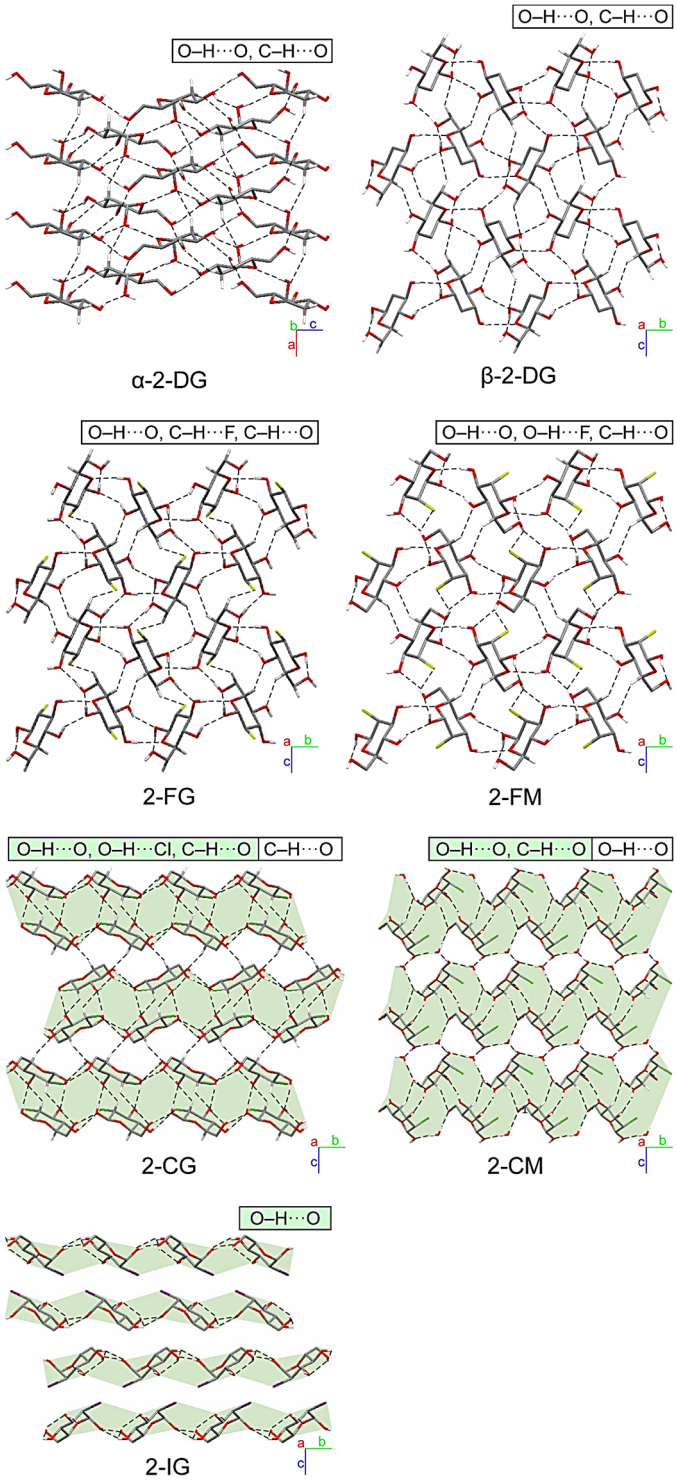

Figure 4. Comparison of packing of molecules in the crystals of investigated halogenated derivatives of glucose and mannose, and the α- and β-anomers of their parent compound. Hydrogen bonds are represented by the dashed lines. The H-atoms not participating in intermolecular hydrogen bonds have been omitted for the sake of clarity. Layered entities have been highlighted in light-green.

An increase in the halogen substituent volume leads to the appearance of more evident changes in crystal packing. It is clear that the H-bond pattern in the crystal lattice of all analysed Cl- and I- derivatives is significantly different from the patterns observed in the compounds described previously. Namely, in the case of derivatives bearing either a Cl or I atom, layered entities spreading along the (101) plane can be distinguished (Figure 4). In the crystal

structure of β-2-CG, molecules are organized in bilayers. Those within this supramolecular assembly are held together by the O−H···O H-bonds (d(D···A) = 2.683(3)−2.771(3) Å; <(D−H···A) = 164(3)−172(3)°)), O−H···Cl (d(D···A) = 3.321(2) Å; <(D−H···A) = 167(2)°) and weak C−H···O H-bonds (d(D···A) = 3.237(3) Å; <(D−H···A) = 128°)) hydrogen bonds (Table S20).The weak C-H . . . O interactions involving the adjacent molecules from neighbouring bilayers stabilises the whole crystal structure (d(D···A) = 3.485(3) Å; <(D−H···A) = 157°; Table S20) of contacts. In the case of the chlorinated mannose derivatives (2-CM), sugar molecules are also arranged in bilayers. However, these layered entities also incorporate water molecules. Within the bilayer, adjacent sugar molecules interact with themselves *via* the O−H···O (d(D···A) = 2.663(3)−2.815(2) Å; <(D−H···A) = 161(4)−168(3)°) and C−H···O (d(D···A) = 3.496(3) Å; <(D−H···A) = 157°) hydrogen bonds, and by the O−H···O (d(D···A) = 2.727(2) Å; <(D−H···A) = 175.3(19)°) interactions with the neighbouring water molecules (Table S23), and these water molecules are also linked by the O−H···O (d(D···A) = 2.629(2) Å; <(D−H···A) = 165(3)°; Table S23) hydrogen bond. Finally, the 2-CM and water molecules from neighbouring two-component layers are interacting by the intermolecular O−H···O (d(D···A) = 2.851(2) Å; <(D−H···A) = 171(3)°; Table S23) interactions. It is worth mentioning that in this structure, no hydrogen bonds involving the halogen atoms were identified. This could be associated with the presence of water molecules in the crystal network, which may be better acceptors for H-atoms in this supramolecular framework.

As mentioned earlier, 2-IG is the only compound among investigated derivatives of 2-DG that crystallised as an α-anomer; however, its supramolecular architecture significantly differs from that observed for α-2-DG (Figure 4). In the case of the iodo-derivative, the molecules are arranged in distinct layers wherein the O−H···O H-bonds (d(D···A) = 2.648(9)−3.169(9) Å; <(D−H···A) = 127(8)−167(11)°; Table S21) between adjacent α-2-IG molecules were identified. However, the framework of intermolecular interactions in α-2-DG is more complex. In this case, adjacent molecules are held together via a dense network of O−H···O (d(D···A) = 2.670(2) − 2.784(2) Å; <(D−H···A) = 155−174°) and C−H···O (d(D···A) = 3.344(3)−3.390(3) Å; <(D−H···A) = 142−148°) hydrogen bonds (Table S17 (ESI)), which leads to the creation of a complex three-dimensional supramolecular assembly [33]. Another aspect of the analysis of the supramolecular landscape was the value of packing indices. Comparison of these values for investigated compounds (69.29-α-2-DG; 68.19%-β-2-DG; 70.07-2-FG; 71.27-2-CG; 71.82%-2-IG; 69.77-2-FM and 70.65%-2-CM) revealed the existence of a subtle trend. Here, the increasing value of packing indices correlated with the increasing volume of the substituent. This finding strongly suggests that in the case of halogenated derivatives of 2-DG, the presence of a more bulky substituent leads to a more efficient filling of space in the lattice.

2.5. Hirshfeld Surface Analysis

Hirshfeld surfaces (HS) of molecules in the crystalline state are calculated by partitioning the electron density in the crystal to obtain such a surface where the contribution to the electron density of the crystal from the sum of spherical atoms of a given molecule (promolecule) starts to prevail over the contribution from others molecules in the crystal (procrystal). In other words, for each point belonging to the HS, the contribution to electron density from the promolecule and procrystal is the same. The useful parameters that enable the mapping of interatomic distances are d_i and d_e, which show the closest distance from a point on the HS to an atom nucleus located inside or outside the surface. A convenient way to visualize intermolecular contact in the crystal lattice is to use a two-dimensional fingerprint plot, describing the relation of d_i to d_e for each point on the Hirshfeld surface, highlighting differences in the crystal lattice among the structures to compare. Furthermore, HS analysis provides a quantitative description of intermolecular interactions in the lattice, allowing the contribution of each type of interatomic contact to the global interaction pattern in the crystal structure. All fingerprint plots are shown in Figure 5, whereas the HS are presented in Figure S4.

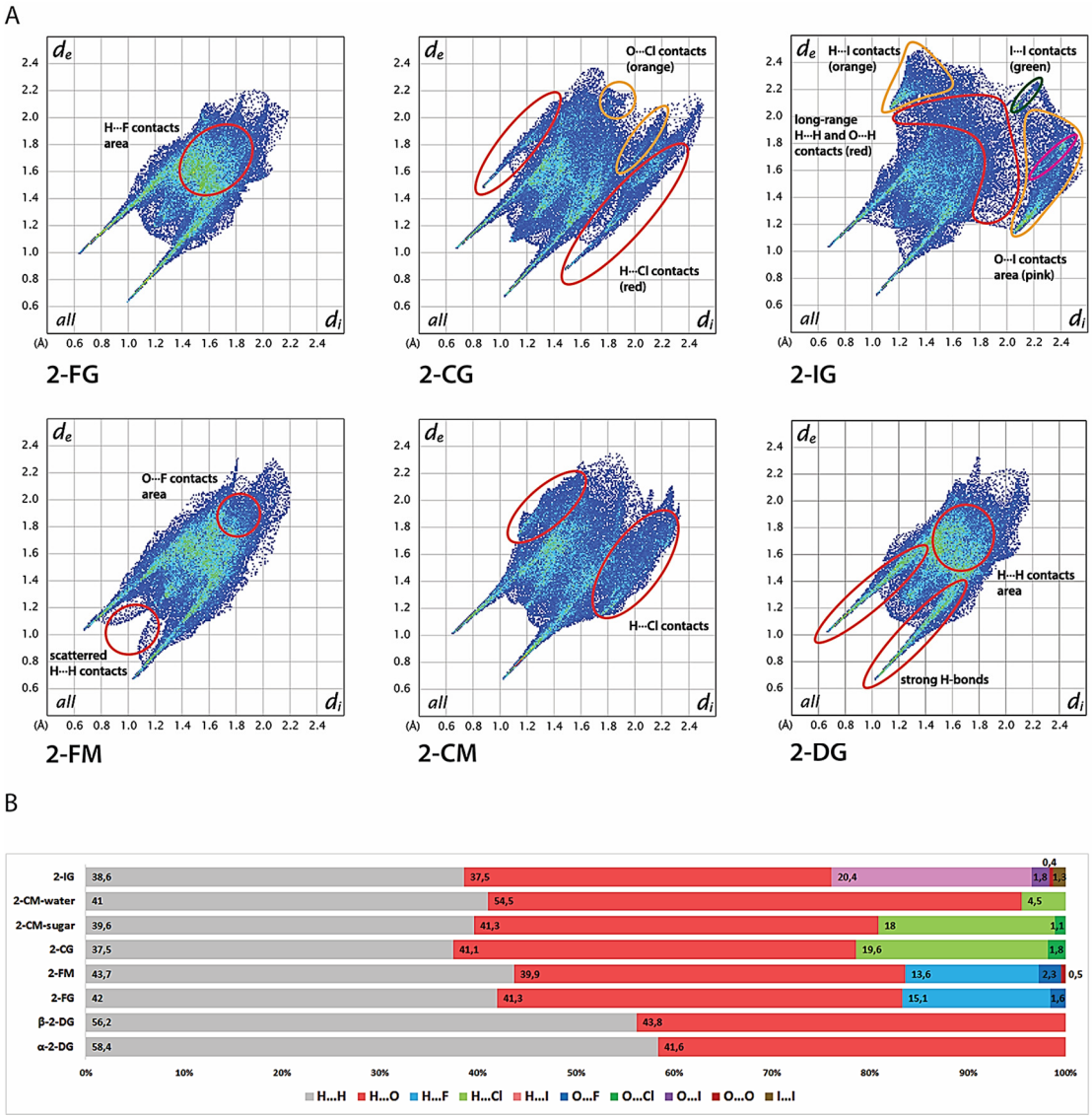

Figure 5. Hirshfeld analysis of the crystal structures. (**A**) Two-dimensional fingerprint plots for the analysed crystals. (**B**) Contribution of each type of interatom contact to the overall Hirshfeld surface for each crystal lattice.

The most distinguishable features of both 2-DG and its halogen derivatives are characteristic, diagonally-symmetric, sharp "spikes," which confirm the existence of strong O-H···O hydrogen bonds to overall interatomic contacts in the crystal lattice (average estimated sum of d_i and d_e is from 1.6 to 2.8 Å for all compounds). The location and directionality of the edges are virtually the same for 2-DG and its derivatives, which indicate that halogen substitution does not alter the global pattern of close O···H contacts in the lattice. Furthermore, the substitution is also not significant in terms of contribution of O···H contacts to the HS, which oscillate near 40%. The only minor exception is 2-IG, where the percentage of O···H contacts is 37.5%. For unsubstituted structures, the contribution of H···H contacts is 58.4% and 56.2% for α- and β-2-DG, respectively. In contrast, the introduction of a halogen atom reduces the percentage of O···H contacts starting from 41.3% (2-FM and 2-CM) to 37.5% (2-IG) in favour of X···H contacts. The lowest contribution is observed for fluorine (13.6%-2-FM and 15.3%-2-FG); for chlorine the contribution is increased (18%-2-CM and 19.6%-2-CG), achieving the highest percentage of 20.6% for 2-IG. This observation is mostly related to the increasing size of the halogen substituent. Moreover, fingerprint plots of 2-CG and 2-CG show a high number of longer ($d_i + d_e > 3.5$ Å) O···H and H···H contacts, which stipulate slightly dense crystal packing, and this tendency

is even more pronounced in the case of 2-IG. The contribution of other contacts, namely, O···O, O···X, and X···X, is mostly marginal. These contacts are rather long-range and do not play an important role in the lattice. A somewhat surprising finding is the almost total lack of any halogen-halogen only contacts in the investigated structures except for minor I···I interaction in 2-IG. Still, their contribution is minimal (below 1.5%).

The shapes of fingerprint plots for 2-DG and its fluorine derivatives bear a strong resemblance, mirroring their isostructural crystal lattices. The only discernible difference among those compounds is the presence of scattered, medium-range ($d_i + d_e > 2.3$ Å) H···H contacts in 2-FM. Otherwise, the patterns of H···H contacts overlap each other in both F-derivatives and do not differentiate from the H···H contact pattern in both anomers of 2-DG. These observations are in line with the literature showing that, in general, fluorine is considered to be a good mimic of hydrogen in the crystalline state. Both 2-FG and 2-FM form several medium-range H···F contacts scattered in the center of the fingerprint and overlapping with H···H contacts. The presence of secondary "spikes" of H···Cl contacts in the fingerprint plot for 2-CG indicates the presence of relatively strong O-H···Cl bonding between sugar molecules, and the edges of the spikes are around $d_{H\cdots Cl} \approx 2.3$ Å. This feature is less pronounced in the case of 2-CM, where H···Cl interactions are significantly longer and the shortest H···Cl contacts are around 2.8 Å. The shape of the fingerprint for a water molecule in 2-CM confirms strong O-H···O bonding, and only a minimal contribution of H···Cl contacts.

2.6. Cohesive Energies and Energy Frameworks

Total cohesive energy for each compound has been calculated using the *Crystal09* software package (Table 1).

Table 1. Cohesive energies for 2-DG and its derivatives.

Compound	Total Energy (kJ mol^{-1})
α-2-DG	−197.10
β-2-DG	−215.00
β-2-FG	−217.56
β-2-FM	−240.25
β-2-CG	−208.16
β-2-CM	−295.89
α-2-IG	−199.70

In the series of Glc derivatives, the energy slightly increases with the increasing size of the substituents, which shows that a steric hindrance introduced by a halogen atom leads to slight destabilization of the lattice. Nevertheless, this effect is not very noticeable. The total energy for 2-DG and 2-FG (β-anomers) is almost the same and this finding is consistent with their isostructurality. Interestingly, our calculations showed that the cohesive energy of α-2-DG is slightly higher than its second anomer, which indicates lower stability of this form and the observable tendency for this class of pyranoses to crystallize as β anomers. The only exception is 2-IG, where a bulky substituent forces the preference toward an α anomer. It is difficult to discuss the differences in stability between anomers of studied compounds owing to the limited data that are available. However, both α anomers have higher energies than other compounds that crystallize as β anomers, which may indirectly suggest generally higher stability of β anomer in the crystal state. Interaction energies between molecules in the lattice and overall energy frameworks have been calculated using *Crystal Explorer* (Figure 6). In any case, given sugar molecules are involved in several different interactions within a cluster of adjacent molecules. Most of the interaction is mediated by H-bonds, involving halogen atoms (either F or Cl). The isostructurality of β-2-DG and its F-derivatives is manifested in the dimer interaction energies extracted from *Crystal Explorer* calculations (see Table S25). Most energetically important dimers are created (symmetry relation $-x+1, y-\frac{1}{2}, -z+\frac{1}{2}$) via O5···HA(O3) and O1···H4(O4)

H-bonding, and another significant contribution to lattice energy is from O6···H1(O1) and O3···H6(O6) bonds (symmetry relations are $x - 1$, y, z and $-x + 3/2$, $-y + 1$, and $z + \frac{1}{2}$, respectively).

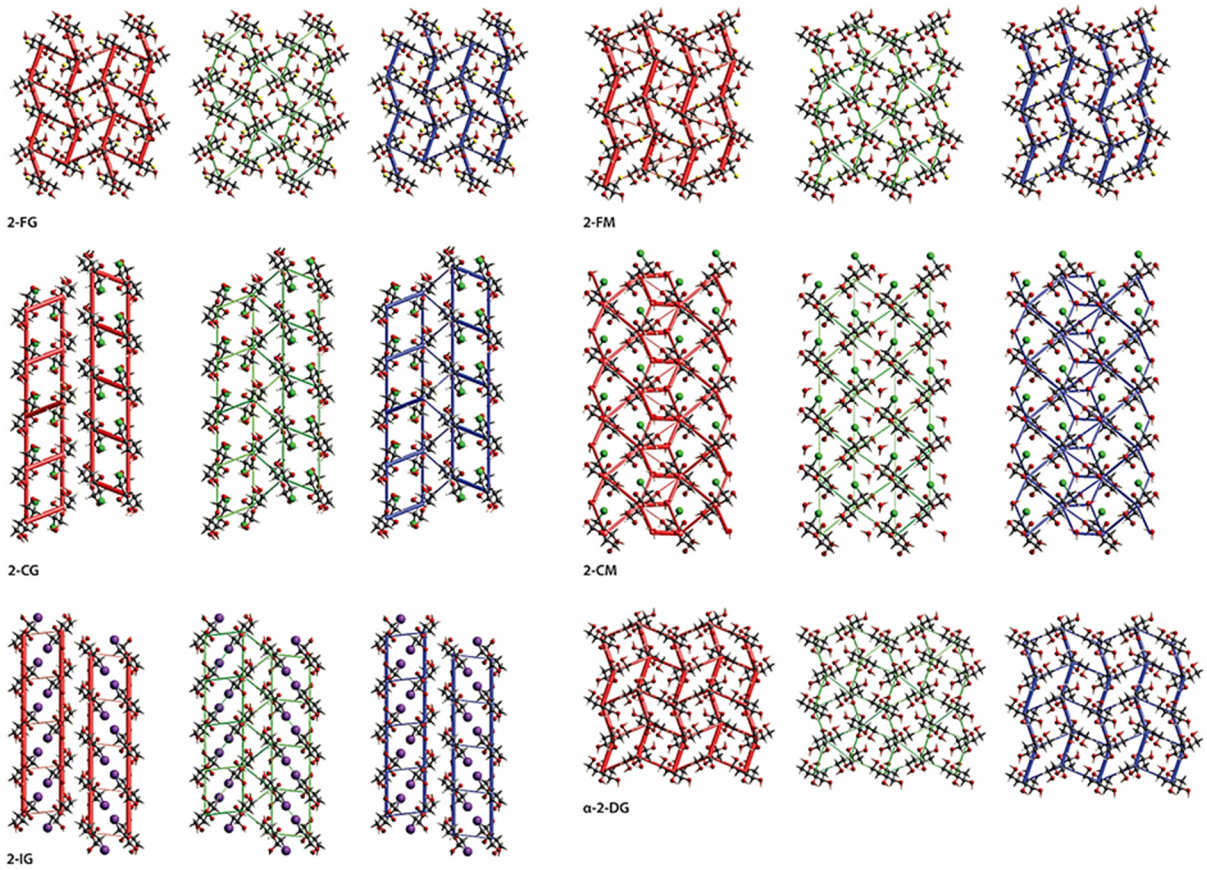

Figure 6. Energy frameworks viewed along *a* direction for the electrostatic (red) and the dispersion (green) components and the total interaction energy (blue).

The directionality and general pattern of these energy frameworks were very similar (Figure 6). Interestingly, additional stability of 2-FM is likely to be caused by the F1···H6(O6) bond, which is not present in 2-FG. In the latter structure, H-F interactions are limited to a relatively weak F1···H6(C6) bond, which is also visible on corresponding Hirshfeld surfaces and fingerprint plots (Figures S1 and S2). The energy framework calculated for *α*-2-DG is also dense. However, it displays different directionality, which is directly caused by different H-bonding geometry in the lattice. The most important contribution is from H-bonds O6···H4(O4) and O5···H1(O1).

The lattice of 2-CG is mostly stabilized by H-bonding involving the C1, C3, and C6 hydroxyl groups, which forms a relatively dense network of interactions leading to the formation of a bilayered supramolecular entity. A somewhat exotic Cl···H6(O6) bond provides only a minor contribution to lattice stabilization. The bilayers are held together mainly by weak dispersive C···H interactions. Due to the presence of water, the energy framework for 2-CM is denser and, to some extent, bears a resemblance to frameworks calculated for 2-FG and 2-FM. As in the case of most hydrates, water-sugar interactions contribute significantly to lattice stabilization. H-bonds O5···H3(O3) and O4···H6(O6) along the a-axis provide the most crucial contribution to stabilization energy. Bilayers interact with one another via O3···H4(O4) and O6···H4(C4) bonds, which are less energetically significant and the latter of which is more dispersive if compared to other H-bonds in the lattice. Owing to substantial steric hindrance related to the iodine atom, the energy framework for the 2-IG lattice is predominantly excluded from interactions

within 2-dimensional monolayers. The most significant contributions are from x ± 1, y, z, dimers (O5···H3(O3) and O3···H6(O6) bonds) and, to a lesser extent, x, y ± 1, z dimers, which form other H-bonds. Interactions between the monolayers are much weaker and are mediated by H···H and H···I contacts, and a significant energetic contribution is from the dispersive term. In addition to the mentioned studies, we also calculated the enrichment ratios (E_{XY}) for interatomic contacts whenever they were statistically significant. In all compounds the E_{OH} was higher than 1.0, which is caused by the formation of energetically favourable H-bonds. A similar trend was evident for hydrogen-halogen contacts where E_{XH} was also higher than 1, indicating that halogen is preferred in contacts with H atoms, which is preferred from an electrostatic (F, Cl) or dispersive (I) point of view (see Table S26 for details). These findings further strengthen previously mentioned observations from general analysis of HS and energy frameworks.

2.7. Structure in Aqueous Solution

Apart from the compounds mentioned before in the study, we also included 2-deoxy-2,2-difluoro-D-glucopyranose (2,2-diFG) and 2-deoxy-2-iodo-D-mannopyranose (2-IM) to gain better insight into how the halogen substitution at C2 may alter the conformation of the pyranose ring as well as anomeric and rotamer equilibria.

Due to the endo-anomeric effect, caused mainly by electrostatic dipole-dipole interactions between the O1 and O5 oxygens, the axial (*α*) anomer's contribution is higher than would be expected from simple conformational analysis [34,35]. For the non-modified glucose and mannose in their pyranose forms, the contribution of the *α*-anomer is 37% and 69%, respectively [36]. It is known that preference for axial orientation of the C1 substituent in D-glucopyranose tends to increase along with increased electronegativity of the mentioned substituent. Nevertheless, the nature of a substituent and configuration in the C2 position also influences the magnitude of the anomeric effect [37]. In the case of our glucose derivatives, the impact of halogen substitution in the C2 position is visible only for fluorine-substituted compounds; this is due to the very high electronegativity of fluorine (see Table S27).

Due to the presence of a CF_2 moiety at the C2 position, this effect is more significant for 2,2′-FG than for 2-FG, and the contribution of the α-anomer is 43% and 68%, respectively. In this regard, 2,2′-diFG behaves as an mannose derivative. The prevalence of an energetically unfavoured α-anomer in mannopyranose results from bisection of the torsional angle between the C1-O1 and C1-O5 bonds by the 2'OH group. This so-called Δ2 effect introduces an additional dipolar interaction, which increases the overall electronic destabilization in the pyranose ring, leading to a higher anomeric effect [38]. Because 2-DG is devoid of that OH group, the steric torsion is alleviated, and the α-anomer contribution is reduced to 49%. In contrast to the mentioned glucose derivatives, electronegativity seems to have little influence on anomeric equilibria in mannose derivatives. A more important factor is the size of a substituent. More bulky halogen atoms cause significant steric torsion, which competes with the dipolar effects shifting the equilibrium toward the β-anomer [39].

In an aqueous solution, pyranosides exist as a mixture of $^1C_4$ and $^4C_1$ conformers. However, in most situations, the equilibrium is strongly shifted toward the more energetically stable $^4C_1$ isomer. Several other, less energetically stable conformations may also exist in solution, and the conformational equilibria may be quite intricate [34]. To gain better insight into the studied compound's behaviour in an aqueous solution, we employed NMR spectroscopy to collect both 1D ^1H and ^{19}F spectra and ^{13}C HSQC and NOESY correlation spectra.

$^3J_{H,H}$ constants in the studied compound were derived from either HSQC or ^1H spectra (see Tables S28 and S29 for additional data on ^{19}F spectra), which allowed us to determine most of the H-C_X-C_Y-H torsion angles in the pyranose ring using the expanded Altona equation, which takes into account electronegativity of the neighbouring substituent (see Material and Methods for the details) [40]. The results summarized in Table S27 indicate that all studied compounds exist mostly in the strongly prevalent $^4C_1$ conformation. These

findings were supported by H-H distances calculated from the NOESY spectra. Due to the somewhat limited accuracy of a simple conformational analysis based on exclusively $^{3}J_{H,H}$ constants and ^{1}H NOE data, we were unable to estimate the contributions of other possible conformers (i.e., $^{1}C_{4}$ or twisted chair) or acyclic form. The differences in the pyranose ring geometry between 2-DG and its derivatives are minimal, mostly limited to H1-C1-C2-H2 and H2-C2-C3-H3 torsion angles, which are directly influenced by the substituent. These deviations slightly correlate with the halogen atom size but do not alter the overall geometry of the ring. Conformations in crystal state and in solution also display high similarity. The observed differences are mostly caused by intermolecular H-bonds and dispersive interactions in the crystalline state, which play only a marginal role in the aqueous solution. Observed differences in the H-H distances between solution and crystal structures are caused mostly by two factors. Firstly, the structure in solution is more dynamic. As various conformations are adapted in a fast-exchange regime, for both NOESY factors and scalar coupling values the population-averaged values are observed, hence only an average picture of the conformation is available. Due to the CH_2OH group's free rotation in solution, it is especially pronounced for the distances between H4-H5 and H5-H6 protons whose positions are fixed for the crystal structures. Secondly, the C-H bond length in the crystal structures solved by X-ray is, in most cases, shorter than determined by high-precision spectroscopic methods or neutron diffraction (0.97 Å *vs* 1.09 Å on average). The difference is caused by the independent atom model (IAM) limitation in the structure refinement in X-ray crystallography [41]. Even if this difference is considered in the data normalization in the NOE analysis, the moderate precision in determining H-X bond in IAM refinement may hinder the conformational analysis.

To estimate the relative distribution of the *gt*, *gg*, and *tg* C5-C6 rotamers, we applied formalism proposed by Stenutz et al. derived from analysis of $^{1}J_{CH}$, $^{2}J_{HH}$, and $^{3}J_{HH}$ coupling constants using limiting values for $^{3}J_{H5,\,H6R}$, $^{3}J_{H5,\,H6R}$, and $^{2}J_{H6R,\,H6S}$ derived from a set of general Karplus equations (see Materials and Methods for details) [42]. Their position within the pyranose ring halogen substitution has no measured effect on the rotamer population compared to the parent compound. On the other hand, a slightly higher contribution of the *gt* is observed for the β anomer for each of the halogenated analogues and 2-DG. Nonetheless, these apparent differences approach the accuracy of the conformational analysis. Without more detailed studies beyond the scope of this work, it is unlikely to provide a definitive explanation of this phenomenon. We did not observe any structural disorder in the crystal structure that may indicate any other rotamers than reported in Table S27. The existence of a given rotamer is imposed merely by the crystal packing and a network of H-bonding in the crystal lattice. It may be different from the rotamer equilibria in solution.

2.8. Protein-Ligand Interaction

Since there are several protein-ligand (15 January 2021) complexes containing 2-FG in the PDB database, we were interested in unravelling some details involving the nature of protein-ligand interactions in these structures, including mapping of interatomic contacts as well as electrostatic interaction energies (E_{el}). We selected a few exemplary structures using the following criteria: conformation similar to that existing in the solid and aqueous states, lack of covalent bonds with the macromolecule or other ligands, and high quality of the structure, especially for the catalytic centre. We decided to focus on point mutants of fungal pyranose 2-oxidase (P2Ox) participating in lignin degradation by producing H_2O_2, which is needed for peroxidases involved in lignin metabolism [43]. P2Ox oxidizes aldopyranoses derived from cellulose and hemicellulose at the C-2 or C-3 position to the corresponding ketoaldolases [44]. The 2-FG is a slow substrate for this enzyme; hence it found some application in its biochemical and structural characterization [45–47]. Since the wild-type structure with 2-FG is not available, we decided to use F454N mutants because this residue is not directly involved in substrate binding. In the F454N mutant, the 454N residue does not interact directly with the substrate and thus does not contribute to binding

energy, whereas 454F in the other structure displays the same behaviour. Nevertheless, the substitution leads to the substrate loop's increased flexibility, which may indirectly affect the binding [46].

The catalytic centre structure and most notable protein-ligand interactions are depicted in Figure 7A. Structural alignments of all protein structures showed an overall high degree of similarity between them regarding the catalytic centre (Figure S4), which was mentioned previously [46,47]. In all investigated complexes, 2-FG exists in the $^4C_1$ conformation, and the geometry of the pyranose ring is very similar in each structure. Moreover, these geometries also show similarity to the structure present in the crystalline state, except for different anomeric forms (Figure 7B).

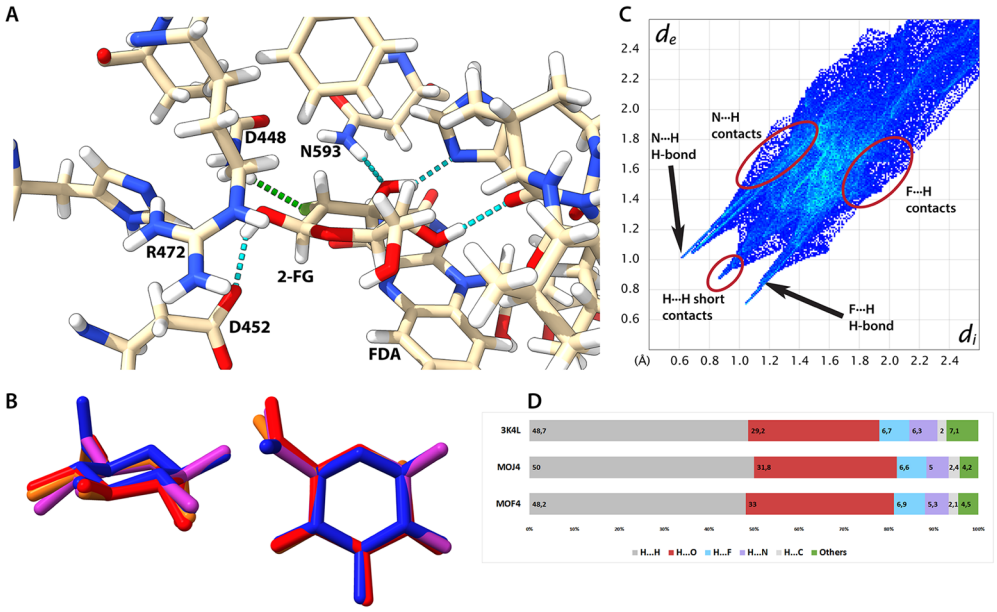

Figure 7. Interactions between 2-FG and selected mutants of P2Ox. (**A**) Structure of catalytic centre of 3K4L structure (some residues have been removed for the sake of ligand visibility). Canonical H-bonds are depicted as dotted cyan lines and F-H bond is depicted as a green dotted line. Residues having a substantial contribution (both negative and positive) to binding are labelled. (**B**) Superimposed structures of 2-FG from 3K4L (magenta), MOJ4 (red), and MOF4 (orange) compared to the structure from the crystalline state (blue). (**C**) Fingerprint plot for the complexed 2-FG in 3K4L structure. (**D**) Contribution of different X···X contacts for 2-FG protein complexes derived from their Hirshfeld surfaces.

To achieve an in-depth understanding of interaction in macromolecular structures, charge-density distribution, which may be computed using several quantum-mechanical approaches for small molecules, was taken into account. Then, charge density distribution can be transferred to bigger molecules, e.g., proteins. These methods assume that atoms located in similar chemical environments have similar charge density distributions, which can be emulated by a set of aspherical pseudoatoms. We decided to use a University at Buffalo Pseudoatom Databank (UBDB) composed of theoretically derived pseudoatoms assigned to corresponding atoms in the ligand and protein. It allowed us to obtain E_{el}. using the exact potential and multipole model (EPMM). We then calculated ligand-interaction energies for each amino-acid residue and then focused on selected residues located near the ligand molecule (Table 2).

The aims were (1) to find which residues contribute the most to binding and compare our finding with qualitative analysis in the literature, and (2) to check whether these interaction energies are relevant to some macroscale kinetic or thermodynamic parameters such as Michaelis constants (K_m), which were determined previously (Table 3).

Table 2. Electrostatic interaction energies (kJ mol^{-1}) between 2-FG and residues in the binding pocket for chosen ligand-protein complexes. A type of point mutation(s) is provided in parentheses.

Residue Type	Number	Interaction Energy [kJ mol^{-1}]		
		3K4L (F454N)	4MOF (H450G)	4MOJ (H450G/V456C)
T	169	−56.0	−144.3	−140.3
A	171	−22.5	−22.3	−24.9
L	361	−26.7	−27.9	−30.8
Q	448	−73.4	−47.6	−55.9
H [a]	450	+11.5	−3.4	−3.2
D	452	+419.1	+431.7	+494.5
R	472	+449.2	−440.6	−497.2
F	474	−53.1	+86.0	−59.4
L	545	+48.7	+34.0	+53.0
V [b]	546	−19.3	−38.7	−32.7
H	548	−35.3	−5.6	−24.1
N	593	−160.3	−131.2	−155.3
FDA [c]	801	−103.5	−188.9	−163.7
SUM		−512.3	−490.0	−635.1

[a] replaced by G in 4MOF and 4MOJ. [b] replaced by C in 4MOJ. [c] dihydroflavine-adenine dinucleotide.

Table 3. Kinetic parameters (with D-glucose as electron donor and O_2 as electron acceptor) of P2Ox mutants compared to the total interaction energy between protein and 2-FG.

Parameter [a]	3K4L	4MOF	4MOJ
Total E_{el} [kJ mol^{-1}]	−512.3	−490.0	−635.1
Michaelis constant (K_m) [mM]	1.5 ± 0.1	0.939 ± 0.04	2.43 ± 0.27
Turnover number (k_{cat}) [s^{-1}]	12.0 ± 0.0	12.5 ± 0.2	16.8 ± 0.27
Specificity constant (K_m/k_{cat}) [mM s^{-1}]	8.2	12.7	13.5

[a] parameters were taken from the literature [44,45].

The most significant contribution to binding energy comes from R472, which is not involved in direct H-bonding However, it shows that the negatively charged FDA molecule influences charge density distribution in the ligand with a formal neutral charge. Therefore, low *E*el for this residue is a consequence of charge redistribution from FDA to 2-FG. It also explains the finding of the repulsive character of D452 interactions, which form an H-bond with the ligand. In this case, it may be explained by electrostatic and steric factors since the localization of the residue in the binding cavity impedes the ligand's preferable geometry. A similar situation is observed for the FDA, where flavin interacts with the 4OH group and H atoms in the pyranose ring. The contribution of other amino-acid residues is less significant. It comes from strong H-bonds (Q448, V546, H548, and N593) or medium- to long-range interactions of a dispersive character as H···H (F474, L361) or C-H···O (T169) contacts. The destabilizing effect of H450 and L545 is predominantly caused by H···H and H···O repulsive interactions, respectively. Comparison between interaction energies among P2Ox mutants shows that only in double mutants the energy is significantly lower, and there is no evident correlation between interaction energy and kinetic parameters. However, it needs to be mentioned that K_m and k_{cat} are kinetic parameters showing the concentration of the substrate, in which half of the maximal reaction velocity and the maximum conversion of the substrate molecules per second (for a single catalytic site) can be achieved. On the other hand, the dissociation constant (K_d) is a thermodynamic parameter directly showing the affinity of a ligand to its molecular target and the relationship between the parameters mentioned above. Unfortunately, values of K_d for 2-FG to P2Ox are not available in the literature, which obfuscates a more detailed analysis of the relationship between E_{el} and ligand-protein interactions in this case.

Using a different approach to study ligand-protein interaction for all structures, we generated HS and fingerprint plots for 2-FG bound in the catalytic centre (Figure 7,

Figures S4 and S5). We included the same residues that were discussed in the previous paragraph (Table 3). The distributions of interatomic contacts are the same for each structure (Figures S4 and S5), showing that one or two single substitutions have negligible effects on the interaction patterns, hence the following discussion concerns all studied complexes. A fingerprint plot for the 3K4L structure is depicted in Figure 6C; the pattern of contacts is similar when compared to the crystalline state (see Figure S4). The main difference is a high number of long-range interactions in the protein complex caused by the less dense packing and the removal of water molecules before interaction energy calculations. Otherwise, the shapes of the fingerprint are very alike in both instances because the most important contributions come from H-bonding and H···H short contacts. The nature of H-bonds in the complex (rendered as a dotted line in Figure 6B) stemmed from different chemical compositions of the adjacent residues (see Table S30 for details). In three H-bonds, the donors are within the 2-FG molecule (O1, O3, and O4) and interact with the COO- group of D452, C=O group of V546, and nitrogen atom from the histidine ring of H548, respectively. The O3 atom in FG-2 is an acceptor of an H-atom belonging to the NH_2 group of N593. Interestingly, a fluorine atom is involved in H-bonding, acting as an acceptor of an H atom from the NH2 group of Q448. This H-bond was not recognized in the previous literature, and its existence explains the relatively high contribution of Q448 to the total interaction energy. Due to the presence of strong N-H hydrogen bonds, the percentage of N···X contacts between 2-FG and its surroundings is relatively high, and the contribution of O···H contacts is reduced if compared to the solid-state crystalline structure. Another difference is a higher contribution of H···H contacts in the complex, which is mostly caused by the presence of H-rich aliphatic fragments and aromatic rings in the vicinity of the ligand.

3. Materials and Methods

3.1. X-ray Data Collection and Structure Refinement

Good-quality single-crystals of 2-FG, 2-CG, 2-IG, 2-FM, and 2-CM were selected for the X-ray diffraction experiments at T = 100(2) K. Diffraction data were collected on the Agilent Technologies SuperNova Dual Source diffractometer with Cu$K\alpha$ radiation (λ = 1.54184 Å) using CrysAlis RED software (CrysAlisPRO, Oxford Diffraction/Agilent Technologies UK Ltd., Yarnton, England). In all cases, the analytical numerical absorption correction using a multifaceted crystal model implemented in SCALE3 ABSPACK scaling algorithm, was applied [48]. The structural determination procedure was carried out using the SHELX package [49]. The structures were solved with direct methods and then successive least-square refinement was carried out based on the full-matrix least-squares method on F^2 using the SHELXL program. All hydrogen atoms linked to oxygen atoms were located from the Fourier difference electron density maps and refined with U_{iso}(H) = 1.5O_{eq}(O). The DFIX 0.82 and 0.85 restraints were applied respectively for the O−H distances of hydroxyl groups of sugar and water molecules. The distance between adjacent H-atoms within the water molecule in 2-CM was restrained to 1.39 Å. All remaining H-atoms were positioned geometrically, with C–H equal to 0.97 and 0.98 Å for the methylene and methine H-atoms, respectively, with U_{iso}(H) = 1.2 U_{eq}(C). All molecular interactions in the crystals of the investigated compounds were identified using the PLATON program [50]. The figures for this publication, regarding the structures in the crystalline state, were prepared using the Olex2 and Mercury programs [51,52].

3.2. Hirshfeld Analysis and Crystal Lattice Energy

The optimizations of the molecular geometries at fixed lattice parameters of -F, -Cl, and -I derivatives were performed using *Crystal09* with the DFT method and B3LYP functional [53]. We applied 6–31 G(d,p) basis set [54] for H, C, N, and O and pob-TZVP basis set [55,56] for F, Cl, and I atoms. The crystal lattice energies were calculated with Grimme dispersion [57,58] and BSSE corrections available in the used version of the software and according to the manual provided by the software developer (Crystal Solutions) [59]. Energy

frameworks were calculated with the B3LYP functional and 6–31 G(d,p) basis set using CrystalExplorer17.5 (University of Western Australia, 2017) [23]. Hirshfeld surfaces [60] and two-dimensional fingerprint plots [61] were also calculated using CrystalExplorer17.5 and the atomic coordinates used in the calculations were taken from the given crystallographic data set. The enrichment ratios of interatomic contacts were calculated accordingly to the literature [62] using the following equations:

$$S_X = C_{XX} + \frac{1}{2} \sum_{Y \neq X} C_{XY} \quad (1)$$

$$R_{XY} = 2S_X S_Y \quad (2)$$

$$E_{XY} = C_{XY} / R_{XY} \quad (3)$$

where C_{XY} is a contribution of a given type of atomic contact to the Hirschfeld surface and E_{XY} is the enrichment ratio.

3.3. Electrostatic Calculations (Ligand-Protein Complexes)

Pseudoatom databanks allowed for the reconstruction of the electron density of macromolecular systems for which experimentally derived geometries are available. In this study, we used UBDB [63] and LSDB to transfer the multiple parameters of the atom types stored in UBDB for the protein-2-FG complexes.

3.3.1. Preparation of the Protein Structures

Molecule 2-FG as a ligand was found in 35 PDB entries [64]. We selected only crystal structures with measured resolution better than 2.5 Å, and G2F as a standalone ligand. After applying selection criteria, pyranose-2-oxidase H450G mutant (pdbid: 4mof), F454N mutant (pdbid: 3k4l), and H450G/V546C double mutant (pdbid: 4moj) were considered for further studies. We first used Reduce software to add hydrogen atoms to water molecules, protein residues, and ligands to optimize the hydrogen bond network for all the analysed PDB structures. Then, water molecules were removed. Arg, Lys, Asp, and Glu residues were treated as ionized. All amino-acid residues and molecules of 2-FG were scaled independently to their formal charges after the databank transfer.

3.3.2. Electrostatic Interaction Energy between Ligand and Protein

To obtain the electrostatic interaction energy (E_{el}) between drug and receptor, the exact potential and multipole model (EPMM) [65] was applied, which allowed computation of E_{el} between two molecular charge distributions represented within the Hansen–Coppens electron-density formalism [66]. It combines a numerical evaluation of the exact Coulomb integral for short-range interatomic interactions (less than 4.5 Å) with a Buckingham type multipole approximation for the long-range contacts. After generating charge density distributions of selected complexes with the aid of the UBDB, the EPMM method was executed in XDPROP [67]. The chains were analysed separately.

3.3.3. Geometry of Ligand Binding and Molecular Visualisation

HS and fingerprint plots for the ligands coordinated by amino-acid residues were calculated in the same manner as for the crystal structures described earlier, starting with the same prepared PDB structures used for electrostatic calculations. All further manipulation of the structures (structural alignments, finding H-bonds, superimposed ligand geometries), as well as images of protein-ligand interactions, were created using UCSF ChimeraX [68].

3.4. NMR Spectroscopy

3.4.1. Data Collection and Processing

All NMR experiments were conducted on a 600 MHz Agilent DD2 spectrometer equipped with a standard 5 mm HCN triple-resonance room temperature probe head. Measurements were performed at a temperature of 298 K. All 1D experiments were displayed and analysed in the MNova (Mestrelab Research) program, and 2D in MNova or UCSF Sparky [69]. For resonance assignment, a set of three experiments for each sample was used (i.e., COSY, ^{13}C-HSQC, and HMBC). For the measurement of scalar coupling constants, two types of experiments were used: ^{1}H 1D spectrum (with water suppression) for well-separated resonances (peaks not overlapping with others) and a modified version of ^{13}C-HSQC (below, called ^{13}C-HSQC-AP) for signals overlapped in a 1D spectrum. The ^{13}C-HSQC-AP was performed with no carbon decoupling during the acquisition period, which allowed for a long acquisition time (of 1.2 s), leading to narrow spectral linewidths, crucial for *J*-coupling determination. The coherence at the beginning of the acquisition time was anti-phase proton magnetization (with respect to carbon). During acquisition time, it was gradually converted into an observable in-phase proton magnetization. Such a scheme allowed us to obtain peaks of a proper phase, independently of the proton-carbon scalar coupling constant used for coherence transfer. Determination of *J*-coupling constants using 1D data sets was performed by line fitting, which allowed us to accurately determine small coupling constants in a case of partially overlapping multiplet components (often observed for pairs of protons at C1 and C2). Determination of *J*-coupling constants using 2D spectra was performed using peak positions, without using any fitting procedure. NOE factors were determined from a set of 2D NOESY experiments for each compound. The set consisted of spectra recorded for six different NOESY mixing time values, i.e., 100, 200, 350, 500, 600, and 750 ms. For each spectrum, cross-relaxation rate constants σ (equal to the slopes of the dependencies of a given correlation peak intensity vs. mixing time) were determined. The distances between nuclei (r) were determined based on a reference distance r_{ref} between the two protons of the methylene group at the C6 atom in the β form of each sugar, assumed to be equal to 1.77 Å (on the base of the geometrical structure of the pyranose ring), using the following formula:

$$r = r_{ref}\left(\frac{\sigma}{\sigma_{ref}}\right)^{-1/6} \quad (4)$$

where σ_{ref} is the cross-relaxation rate of a reference signal. Relevant experimental parameters for all experiments were gathered in Table 4.

Table 4. Experimental parameters for data acquisition for the NMR experiments.

Parameter	COSY	^{13}C-HSQC	HMBC	NOESY	^{1}H	^{13}C-HSQC-AP
Relaxation delay [s]	1	1.5	1	6	1	1.5
Number of transients	4	2	4	4	8	8
Acquisition time [s]	0.15	0.15	0.15	0.15	1.7	1.2
Number of increments	200	300	200	200	n.a.	400

3.4.2. Conformational Analysis

H-C_X-C_Y-H torsion angles in the pyranose ring in the solution were calculated using the following equation:

$$^{3}J_{H,H} = C_0 + C_1cos(\phi) + C_2cos(2\phi) + C_3cos(3\phi) + S_1sin(\phi) + S_2sin(2\phi) \quad (5)$$

where φ is a torsion angle and coefficients C_i and S_i are either numerical constants or functions of relative electronegativities λ_i of substituents in C_X and C_Y atoms themselves. Values of the above-mentioned parameters were taken from the literature [40,70,71], where the detailed derivation of the aforementioned equation and its components is also provided.

C5-C6 rotamer populations were estimated using the following set of linear equations:

$$^{3}J_{H5,H6R} = 9.9A + 0.8B + 4.5C \quad (6)$$

$$^{3}J_{H5,H6S} = 1.5A + 1.3B + 10.8C \quad (7)$$

$$A + B + C = 1 \quad (8)$$

where number coefficients are limiting values of $^{3}J_{H5,H6R}$, $^{3}J_{H5,H6R}$ coupling constants for a given rotamer and parameters A, B, and C are molar fractions of gt, gg, and tg rotamers, respectively.

C6-O6 rotamer populations were estimated using a following set of linear equations:

$$^{2}J_{H6R,H6S(gauche)} = 12.7(A + B) + 11.5C \quad (9)$$

$$^{2}J_{H6R,H6S(trans)} = 9.7(A + B) - 8.5C \quad (10)$$

$$^{2}J_{H6R,H6S(app)} = {}^{3}J_{H6R,H6S(gauche)}D + {}^{3}J_{H6R,H6S(trans)}E \quad (11)$$

$$D + E = 1 \quad (12)$$

where number coefficients are limiting values of $^{2}J_{H6R,H6S(gauche)}$, $^{2}J_{H6,H6S(trans)}$ coupling constants for a given rotamer, A, B, and C are molar fractions of gt, gg, and tg rotamers, respectively, and D and E are molar fractions of *gauche* and *trans* rotamers, respectively. Values of all torsion angles and H-H distances for the crystal structures were calculated in UCSF Chimera [72].

4. Conclusions

Our structural research showed that halogen substitution at the C2 position has a significant effect on the crystal structure of the pyranoses; however, the structure of the ring itself is mostly unaffected by the presence of the halogen atom, which was quantitatively shown using CP parameters. The changes in the crystal structure are mostly caused by steric effects because increasing size of the substituent leads to formation of a layered structure having higher packing indices. In spite of more efficient space filling, the H-bond network is less dense in chloro- and iodine derivatives due to higher volume of the substituent itself. Since fluorine is considered to be a good mimic of both hydroxyl groups and hydrogen in many systems, crystals of both F-derivatives have very similar structure to the β anomer of 2-DG. Neither packing nor pattern of H-bond is altered in any significant way. To achieve more profound effects on crystal structure, it is necessary to introduce more F atoms to the pyranose ring, which has been extensively studied in earlier studies. In some instances, the F or Cl substituent is capable of forming H-bonds as an acceptor, which suggests (in the case of 2-FG and 2-FM) that fluorine is more isosteric with OH groups than with hydrogen atom. We found that Hirshfeld partitioning is a useful tool in the quantitative analysis of interatomic interactions in systems having intricate networks of H-bonds and other short- and medium-range interactions. Our analysis indicates that the general pattern of interatomic interactions is preserved upon halogen substitution; however, some of the H···H contacts in the parent compound are replaced by H···X (where X is a halogen) contacts. The only noticeable alteration is an increasing number of medium- to long-range interactions between H and X, which is positively correlated with increasing volume of X. None of the studied compounds possesses halogen bonds within their crystal structures, even if the halogen atoms are located in the relative vicinity, as in the case of 2-IG. It can be noticed that the major contributions to intermolecular interaction in the structure are attributable to H-bonds and short-range H···H(X) contacts whilst other interactions (i.e., O···X or X···X) are marginal. These observations are further supported by the energy framework calculations showing that strong H-bonds between H and O provide the most substantial contribution to the lattice energy, and the increasing contribution of dispersive term is positively correlated with the size and polarizability of

the substituent. The directionality of the frameworks also confirms the layered structure of Cl and I derivatives, where the mono- or bilayers are composed of strongly interacting molecules but interactions between the layers themselves are relatively weak, mostly dispersive of the H···H or H···X type. Despite the different chemical nature of substituents, the main factor contributing to changes in the crystal structure is the size of the halogen atom, which imposes the formation of a layered supramolecular landscape.

NMR spectra showed similarity between pyranose puckering between 2-DG and the studied derivatives. Introduction of a halogen atom does not impose any significant conformational changes, and all compounds exist in the most stable $^4C_1$ chair conformation. As only averaged NMR parameters are observable, it is difficult to estimate the contribution of minor conformation states or chain structures. However, comparison of the NMR and X-ray data indicates that the structure observed in crystal is predominant also for the respective anomer in solution. To achieve higher precision in the calculation of torsion angles, we applied an extended Karplus-like equation, which takes into account the effects of electronegativity of adjacent substituents. The differences in torsion angles are not significant and stemmed from different chemical environments between solvated molecules in solution and molecules in the crystal; in the latter, the directionality of H-bonds and dispersive interactions play significant roles whereas their roles are negligible in solution. The direct comparison of intramolecular H-H distances between molecules in the crystal state and solution is difficult due to difference in C-O and C-H bonds inferred from spectroscopic and X-ray crystallographic experiments. Nonetheless, our NOESY data also indicate that the $^4C_1$ conformation prevails in aqueous solution. The only significant structural difference among studied compounds (in aqueous solution) was the α/β anomer ratio, which is caused by stereoelectronic effects invoked by halogen substitution.

Using a few chosen PDB structures of P2Ox, we were able to extract interaction electrostatic energies between the 2-FG and protein residues within the binding cavity and thus obtain the overall interaction energy between the ligand and protein. However, due to the lack of data on any thermodynamic parameters (e.g., K_i or ΔH), it was difficult to relate these findings to ligand binding because the calculated energies were similar to one another. Analysis of the Hirshfeld surface showed that the chemical environment of 2-FG in the binding cavity is similar to the one in its crystal structure; we also found that a H-F hydrogen bond plays an important role in the binding, a detail omitted by previous studies on that system.

Supplementary Materials: The following are available online at https://www.mdpi.com/article/10.3390/ijms22073720/s1, Table S1: Crystal data and structure refinement details for the investigated compounds; Table S2: Bond length for 2-FG; Table S3: Values of valence angles for 2-FG; Table S4: Values of torsion angles for 2-FG; Table S5: Bond lengths for 2-CG; Table S6: Values of valence angles for 2-CG; Table S7: Values of torsion angles for 2-CG; Table S8: Bond lengths for 2-IG; Table S9: Values of valence angles for 2-IG; Table S10: Values of torsion angles for 2-IG; Table S11: Bond lengths for 2-FM; Table S12: Values of valence angles for 2-FM; Table S13: Values of torsion angles for 2-FM; Table S14: Bond lengths for 2-CM; Table S15: Values of valence angles for 2-CM; Table S16: Values of torsion angles for 2-CM; Table S17: Cremer-Pople parameters for crystal structures; Table S18: The geometry of hydrogen bonds in the crystal of α-2-DG; Table S19: The geometry of hydrogen bonds in the crystal of β-2-DG; Table S20: The geometry of hydrogen bonds in the crystal of β-FG; Table S21: The geometry of hydrogen bonds in the crystal of β-CG; Table S22: The geometry of hydrogen bonds in the crystal of β-IG; Table S23: The geometry of hydrogen bonds in the crystal of β-FM; Table S24: The geometry of hydrogen bonds in the crystal of β-CM; Table S25: Interaction energies (kJ mol^{-1}) for adjacent molecules; Table S26: The geometry of hydrogen bonds between 2-FG and protein residues for 3K4L structure; Table S27: Conformational analysis of the halogenated analogues of 2-DG in an aqueous solution and in the crystal state; Table S28: ^{1}H-^{13}C HSQC and ^{1}H NMR data for halogenated analogues of 2-DG and the parental compound. NMR shift values are measured in ppm and *J*-coupling constants in Hz; Table S29: ^{19}F NMR data for fluorinated analogues of 2-DG. NMR shifts values are measured in ppm and *J*-coupling constants in Hz; Figure S1: Hirshfeld surfaces mapped onto d_e; Figure S2: Contribution of different X-X contacts for each crystal lattice; Figure S3: A:

Comparison between fingerprint plots between α (left) and β (right) anomers of 2-DG, B: Comparison between Hirshfeld surfaces between these structures (α on the left and β on the right) and their energy frameworks (C) where β anomer is on the top and α in the bottom; Figure S4: Structural alignment of amino-acid residues involving in 2-FG binding in 3K4L (green), 4MOF (blue) and 4 MOJ (pink, top-right) an exemplary Hirshfeld surface calculated for 2-FG in 3K4L complex (top-left) and comparison between fingerprint plots for 2-FG in crystal lattice and different protein-ligand complexes; Figure S5: Different X-X contacts for each protein-ligand complexes. CCDC Deposition Numbers 2063278-2063282 contain the supplementary crystallographic data for compounds described in this paper. These data can be obtained freely via http://www.ccdc.cam.ac.uk/data_request/cif (3 March 2021), by e-mailing data_request@ccdc.cam.ac.uk or by contacting directly the Cambridge Crystallographic Data Centre (12 Union Road, Cambridge CB2 1EZ, UK. Fax: +44-1223-336033).

Author Contributions: Conceptualization and study design, M.Z., W.P., K.W., and B.P.; methodology and software, M.Z., A.Z.-K., S.P., M.M., D.T., W.K., and K.W.; validation, M.Z., A.Z.-K., M.M., D.T., and B.P.; formal analysis, M.Z., K.W., and B.P.; investigation, M.Z, A.Z.-K., M.S., S.P., M.M., and D.T.; resources, M.Z., W.K., I.F., R.Z., S.S., and W.P.; data curation, A.Z.-K. and D.T.; writing—original draft preparation, M.Z. and B.P.; writing—review and editing, M.Z., K.W., W.P., and B.P.; visualization, M.Z., S.P. and D.T.; supervision, K.W. and B.P.; project administration, M.Z. and B.P.; and funding acquisition, M.Z. and B.P. All authors have read and agreed to the published version of the manuscript.

Funding: This work was supported by National Science Centre in Poland (grants No. UMO-2017/25/B/NZ3/00251 and UMO-2017/24/C/NZ1/00366). Grant No. UMO-2017/25/NZ3/00251 was carried out with the cooperation of Professor Waldemar Priebe, UT MD Anderson Cancer Center, where new 2-DG derivatives were designed and synthesized and funded by the sponsor research grant from Moleculin Biotech, Inc. The research was carried out at the Biological and Chemical Research Centre, University of Warsaw, established within the project co-financed by the European Union from the European Regional Development Fund under the Operational Programme Innovative Economy, 2007–2013. The X-ray diffraction data collection was accomplished at the Core Facility for Crystallographic and Biophysical research to support the development of medicinal products. The "Core facility for crystallographic and biophysical research to support the development of medicinal products" project was carried out within the TEAM-TECH Core Facility programme of the Foundation for Polish Science co-financed by the European Union under the European Regional Development Fund.

Institutional Review Board Statement: Not applicable.

Informed Consent Statement: Not applicable.

Data Availability Statement: Not applicable.

Acknowledgments: Paulina Dominiak is gratefully acknowledged for valuable scientific discussions concerning the computational studies

Conflicts of Interest: W. Priebe is an inventor on patents covering new derivatives of 2-DG. He is Chair of SAB and a shareholder of Moleculin Biotech, Inc., CNS Pharmaceuticals, and WPD Pharmaceuticals. His research is in part supported by the sponsor research grant from Moleculin Biotech, Inc. and CNS Pharmaceuticals. I. Fokt and R. Zielinski are listed as inventors on patents covering new analogues of 2-DG, are consultants of Moleculin Biotech, Inc., and are shareholders of Moleculin Biotech, Inc. and CNS Pharmaceuticals. M. Ziemniak and K. Wozniak have been involved as consultants and experts in WPD Pharmaceuticals. B. Pająk is CSO for WPD Pharmaceuticals. The other authors declare no conflict of interest.

References

1. Pajak, B.; Siwiak, E.; Sołtyka, M.; Priebe, A.; Zieliński, I.R.; Fokt, I.; Ziemniak, M.; Jaśkiewicz, A.; Borowski, R.; Domoradzki, T.; et al. 2-Deoxy-D-glucose and its analogs: From diagnostic to therapeutic agents. *Int. J. Mol. Sci.* **2019**, *21*, 234. [CrossRef] [PubMed]
2. Phelps, M.E. *PET: Molecular Imaging and its Biological Applications*; Springer: New York, NY, USA, 2004.
3. Fonti, R.; Conson, M.; Del Vecchio, S. PET/CT in radiation oncology. *Semin. Oncol.* **2019**, *46*, 202–209. [CrossRef] [PubMed]
4. De Castro, M.; Marzabadi, C.H. Preparation and reactions of iodo sugars. *Tetrahedron* **2010**, *66*, 3395–3404. [CrossRef]

5. Fokt, I.; Szymański, S.; Skóra, S.; Cybulski, M.; Madden, T.; Priebe, W. D-Glucose and D-mannose-based antimetabolites. Part 2. Facile synthesis of 2-deoxy-2-halo-D-glucoses and -D-mannoses. *Carbohydr. Res.* **2009**, *344*, 1464–1473. [CrossRef]
6. Lampidis, T.J.; Kurtoglu, M.; Maher, J.C.; Liu, H.; Krishan, A.; Sheft, V.; Szymanski, S.; Fokt, I.; Rudnicki, W.R.; Ginalski, K.; et al. Efficacy of 2-halogen substituted D-glucose analogs in blocking glycolysis and killing "hypoxic tumor cells". *Cancer Chemother. Pharmacol.* **2006**, *58*, 725–734. [CrossRef]
7. Batra, S.; Adekola, K.U.A.; Rosen, S.T.; Shanmugam, M. Cancer metabolism as a therapeutic target. *Oncology* **2013**, *27*, 460–467.
8. Oliveira, G.L.; Coelho, A.R.; Marques, R.; Oliveira, P.J. Cancer cell metabolism: Rewiring the mitochondrial hub. *Biochim. Biophys. Acta* **2021**, *1867*, 166016. [CrossRef]
9. Laussel, C.; Léon, S. Cellular toxicity of the metabolic inhibitor 2-deoxyglucose and associated resistance mechanisms. *Biochem. Pharmacol.* **2020**, *182*, 114213. [CrossRef]
10. Liu, C.C.; Jiang, C.J.; Lavis, A.; Croft, L.; Dong, H.Y.; Tseng, F.; Yang, K.; Tay, H.; Hersey, P.; Zhang, X.D. 2-deoxy-D-glucose enhances TRAIL-induced apoptosis in human melanoma cells through XBP-1-mediated upregulation of TRAIL-R2. *Mol. Cancer* **2009**, *8*, 122. [CrossRef]
11. Sottnik, J.L.; Lori, J.C.; Rose, B.J.; Thamm, D.H. Glycolysis inhibition by 2-deoxy-D-glucose reverts the metastatic phenotype in vitro and in vivo. *Clin. Exp. Metastasis* **2011**, *28*, 865–875. [CrossRef]
12. Parris, G. 2-deoxy-D-glucose as a potential drug against fusogenic viruses including HIV. *Med. Hypotheses* **2008**, *70*, 776–782. [CrossRef] [PubMed]
13. Bojkova, D.; Klann, K.; Koch, B.; Widera, M.; Krause, D.; Ciesek, S.; Cinatl, J.; Munch, C. Proteomics of SARS-CoV-2-infected host cells reveals therapy targets. *Nature* **2020**, *583*, 469–472. [CrossRef]
14. Balkrishna, A.; Thakur, P.; Singh, S.; Dev, S.; Jain, V.; Varshney, A.; Sharma, R. Computional screening approaches for investigating potential activity of phytoligands against SARS-CoV-2. *Res. Square* **2021**. [CrossRef]
15. Niccoli, S.; Boreham, D.R.; Phenix, C.P.; Lees, S.J. Non-radioactive 2-deoxy-2-fluoro-D-glucose inhibits glucose uptake in xenograft tumours and sensitizes HeLa cells to doxorubicin in vitro. *PLoS ONE* **2017**, *12*, e0187584. [CrossRef] [PubMed]
16. Piña, Y.; Decatur, C.; Murray, T.G.; Houston, S.K.; Lopez-Cavalcante, M.; Hernandez, E.; Celdran, M.; Shah, N.; Feuer, W.; Lampidis, T. Retinoblastoma treatment: Utilization of the glycolytic inhibitor, 2-deoxy-2-fluoro-D-glucose (2-FG), to target the chemoresistant hypoxic regions in LH9BETA)T(AG) retinal tumors. *Investig. Ophthalmol. Vis. Sci.* **2012**, *53*, 996–1002. [CrossRef]
17. Zhang, W.; Oliver, A.G.; Serianni, A.S. Co-crystals of 3-deoxy-3-fluoro-α-D-glucopyranose and 3-deoxy-β-D-glucopyranose. *Acta Crystallogr. C Cryst. Struct. Commun.* **2010**, *66*, o496–o498. [CrossRef]
18. Denavit, V.; Lainé, D.; St-Gelais, J.; Johnson, P.A.; Giguère, D. A Chiron approach towards the stereoselective synthesis of polyfluorinated carbohydrates. *Nat. Commun.* **2018**, *9*, 4721. [CrossRef]
19. Linclau, B.; Golten, S.; Light, M.; Sebban, M.; Oulyadi, H. The conformation of tetrafluorinated methyl galactoside anomers: Crystallographic and NMR studies. *Carbohydrate Res.* **2011**, *346*, 1129–1139. [CrossRef]
20. St-Gelais, J.; Côté, E.; Lainé, D.; Johnson, P.A.; Giguère, D. Addressing the structural complexity of fluorinated glucose analogues: Insight into lipophilicities and solvation effects. *Chem. Eur. J.* **2020**, *26*, 13499–13506. [CrossRef]
21. Snider, D.A.; Addicks, W.; Owens, W. Polymorphism in generic drug product development. *Adv. Drug Deliv. Rev.* **2004**, *56*, 391–395. [CrossRef]
22. Censi, R.; Di Martino, P. Polymorph impact on the bioavailability and stability of poorly soluble drugs. *Molecules* **2015**, *20*, 18759–18776. [CrossRef] [PubMed]
23. Turner, M.J.; Thomas, S.P.; Shi, M.W.; Jayatilaka, D.; Spackman, M.A. Energy frameworks: Insights into interaction anisotropy and the mechanical properties of molecular crystals. *Chem. Commun.* **2015**, *51*, 3735–3738. [CrossRef] [PubMed]
24. Koritsanszky, T.S.; Coppens, P. Chemical applications of the X-ray charge-density analysis. *Chem. Rev.* **2001**, *101*, 1583–1628. [CrossRef] [PubMed]
25. Pawlędzio, S.; Makal, A.; Trzybiński, D.; Woźniak, K. Crystal structure, interaction energies and experimental electron density of the popular drug ketoprofen. *IUCrJ* **2018**, *1*, 1150–1156.
26. Krawczuk, A.; Macchi, P. Charge density analysis for crystal engineering. *Chem. Cent. J.* **2014**, *8*, 68. [CrossRef]
27. Macchi, P. Modern charge density studies: The entanglement of experimental and theory. *Crystallogr. Rev.* **2013**, *19*, 58–101. [CrossRef]
28. Bieszczad, B.; Pawlędzio, S.; Polak, K.; Antonowicz, J.; Mieczkowski, A.; Trzybinski, A. Influence of halogen size on the supramolecular and energy landscape of the THF solvates of the halogen derivatives of dianthranilide. *CrystEngComm* **2020**, *22*, 5389–5399. [CrossRef]
29. Cremer, D.; Pople, J.A. A general definition of ring puckering coordinates. *J. Am. Chem. Soc.* **1975**, *97*, 1354–1358. [CrossRef]
30. Maluszynska, H.; Ruble, J.R.; Jeffrey, G.A. The crystal structure of 2-deoxy-D-arabino-hexopyranose at -150°. *Carbohydrate Res.* **1981**, *97*, 199–204. [CrossRef]
31. O'Hagan, D. Understanding organofluorine chemistry. An introduction to the C-F bond. *Chem. Soc. Rev.* **2008**, *37*, 308–319. [CrossRef]
32. Meanwell, N.A. Fluorine and fluorinated motifs in the design and application of bioisosteres for drug design. *J. Med. Chem.* **2018**, *61*, 5822–5880. [CrossRef]
33. Hess, D.; Klüfers, P. 2-deoxy-D-arabino-hexopyranose. *Acta Crystallogr. Sect. E Struct. Rep. Online* **2011**, *67*, o2615. [CrossRef]

34. Widmalm, G. Perspective on the primary and three-dimensional structures of carbohydrates. *Carbohydr. Res.* **2013**, *378*, 123–132. [CrossRef] [PubMed]
35. Kirby, A.J. *The Anomeric Effect and Related Stereoelectronic Effects at Oxygen*; Springer: Berlin/Heidelberg, Germany, 1983.
36. Miljkovic, M. *Carbohydrates*; Springer: New York, NY, USA, 2009.
37. Perrin, C.L.; Armstrong, K.B.; Fabian, M.A. The origin of the anomeric effect: Conformational analysis of 2-methoxy-1,3-dimethylhexahydropyrimidine. *J. Am. Chem. Soc.* **1994**, *116*, 715–722. [CrossRef]
38. Reeves, R.E. The shape of pyranoside rings. *J. Am. Chem. Soc.* **1950**, *72*, 1499–1506. [CrossRef]
39. Horton, D.; Turner, W.N. Conformational and configurational studies on some acetylated aldopyranosyl halides. *J. Org. Chem.* **1965**, *30*, 3387–3394. [CrossRef]
40. Donders, L.A.; De Leeuw, F.A.A.M.; Altona, C. Relationship between proton-proton NMP coupling constants and subsituent electronegativities. IV—An extended Karplus equation accounting for interactions between substituents and its application to coupling constant data calculated by the Extended Huckel method. *Magn. Reson. Chem.* **1989**, *27*, 556–563.
41. Blakeley, M.P.; Hasnain, S.S.; Antonyuk, S.V. Sub-atomic resolution X-ray crystallography and neutron crystallography: Promise, challenges and potential. *IUCrJ* **2015**, *2*, 464–474. [CrossRef]
42. Stenutz, R.; Carmichael, I.; Widmalm, G.; Serianni, A.S. Hydroxymethyl group conformation in saccharides: Structural dependencies of $^{2}J_{HH}$, $^{3}J_{HH}$, and $^{1}J_{CH}$ spin-spin coupling constants. *J. Org. Chem.* **2002**, *67*, 949–958. [CrossRef]
43. ten Have, R.; Teunissen, P.J. Oxidative mechanisms involved in lignin degradation by white-rot fungi. *Chem. Rev.* **2001**, *101*, 3397–3413. [CrossRef]
44. Leitner, C.; Volc, J.; Haltrich, D. Purification and characterization of pyranose oxidase from white rot fungus *Trametes multicolor*. *Appl. Environ. Microbiol.* **2001**, *67*, 3636–3644. [CrossRef]
45. Kujawa, M.; Ebner, H.; Leitner, C.; Hallberg, B.M.; Prongjit, M.; Sucharitakul, J.; Ludwig, R.; Rudsander, U.; Peterbauer, C.; Chaiyen, P.; et al. Structural basis for substrate binding and regioselective oxidation of monosac-charides at C3 by pyranose 2-oxidase. *J. Biol. Chem.* **2006**, *281*, 35104–35115. [CrossRef] [PubMed]
46. Spadiut, O.; Tan, T.-C.; Pisanelli, I.; Haltrich, D.; Divne, C. Importance of the gating segment in the substrate-recognition loop of pyranose 2-oxidase. *FEBS J.* **2010**, *277*, 2892–2909. [CrossRef] [PubMed]
47. Tan, T.C.; Spadiut, O.; Gandini, R.; Haltrich, D.; Divne, C. Structural basis for binding of fluorinated glucose and galactose to *Trametes multicolor* pyranose 2-oxidase variants with improved galactose conversion. *PLoS ONE* **2014**, *9*, e86736. [CrossRef] [PubMed]
48. Clark, R.C.; Reid, J.S. The analytical calculation of absorption in multifaceted crystals. *Acta Crystallogr. A* **1995**, *51*, 887–897. [CrossRef]
49. Sheldrick, G.M. Crystal structure refinement with SHELXL. *Acta Crystallogr. A* **2008**, *64*, 112–122. [CrossRef] [PubMed]
50. Spek, A.L. Structure validation in chemical crystallography. *Acta Crystallogr. D Biol Crystallogr.* **2009**, *65*, 148–155. [CrossRef]
51. Dolomanov, O.V.; Bourhis, L.J.; Gildea, R.J.; Howard, J.A.K.; Puschmann, H. OLEX2: A complete structure solution, refinement and analysis program. *J. Appl. Crystallogr.* **2009**, *42*, 339–341. [CrossRef]
52. Macrae, C.F.; Bruno, I.J.; Chisholm, J.A.; Edgington, P.R.; McCabe, P.; Pidcock, E.; Rodriguez-Monge, L.; Taylor, R.; van de Streek, J.; Wood, P.A. New features for the visualization and investigation of crystal structures. *J. Appl. Crystallogr.* **2008**, *41*, 466–470. [CrossRef]
53. Dovesi, R.; Orlando, R.; Erba, A.; Civalleri, B.; Roetti, C.; Saunders, V.R.; Zicovich-Wilson, C.M. CRYSTAL14: A program for the *ab initio* investigation of crystalline solids. *Int. J. Quantum Chem.* **2014**, *114*, 1287–1317. [CrossRef]
54. Gatti, C.; Cargnoni, F.; Bertini, L. Chemical information from the source function. *J. Comput. Chem.* **2003**, *24*, 422–436. [CrossRef] [PubMed]
55. Peintinger, M.F.; Oliveira, D.V.; Bredow, T. Consistent gaussian basis sets of Triple-Zeta valence with polarization quality for solid-state calculations. *J. Comput. Chem.* **2013**, *34*, 451–459. [CrossRef]
56. Laun, J.; Vilela Oliveira, D.; Bredow, T. Consistent gaussian basis sets of double- and triple-zeta valence with polarization quality of the fifth period for solid-state calculations. *J. Comput. Chem.* **2018**, *39*, 1285–1290. [CrossRef]
57. Grimme, S. Accurate description of van der Waals complexes by density functional theory including empirical corrections. *J. Comput. Chem.* **2004**, *25*, 1463–1473. [CrossRef]
58. Grimme, S. Semiempirical GGA-type density functional constructed with a long-range dispersion correction. *J. Comput. Chem.* **2006**, *27*, 1787–1799. [CrossRef] [PubMed]
59. Boys, S.F.; Bernardi, F. The calculation of small molecular interactions by the differences of separate total energies. *Mol. Phys.* **1970**, *19*, 553–566. [CrossRef]
60. Spackman, M.A.; Jayatilaka, D. Hishfeld surface analysis. *Cryst. Eng. Comm.* **2009**, *11*, 19–32. [CrossRef]
61. McKinnon, J.J.; Spackman, M.A.; Mitchell, A.S. Novel tools for visualizing and exploring intermolecular interactions in molecular crystals. *Acta Crystallogr.* **2004**, *60*, 627–668. [CrossRef] [PubMed]
62. Jelsch, C.; Ejsmont, K.; Huder, L. The enrichment ration of atomic contacts in crystals, an indicator derived the Hirshfeld surface analysis. *IUCrJ* **2014**, *1*, 119–128. [CrossRef]
63. Jarzembska, K.N.; Dominiak, P.M. New version of the theoretical databank of transferable aspherical pseudoatoms, UBDB2011—Towards nucleic acid modelling. *Acta Crystallogr. Sect. A* **2012**, *68*, 139–147. [CrossRef]

64. Berman, H.M.; Westbrook, J.; Feng, Z.; Gilliland, G.; Bhat, T.N.; Weissig, H.; Shindyalov, I.N.; Bourne, P.E. The protein data bank. *Nucleic Acids Res.* **2000**, *28*, 235–242. [CrossRef] [PubMed]
65. Volkov, A.; Koritsanszky, T.; Coppens, P. Combination of the exact potential and multipole methods (EP/MM) for evaluation of intermolecular electrostatic interaction energies with pseudoatom representation of molecular electron densities. *Chem. Phys. Lett.* **2004**, *391*, 170–175. [CrossRef]
66. Hansen, N.K.; Coppens, P. Testing aspherical atom refinements on small-molecule data sets. *Acta Crystallogr. Sect. A* **1978**, *34*, 909–921. [CrossRef]
67. Volkov, A.; Macchi, P.; Farrugia, L.J.; Gatti, C.; Mallinson, P.; Richter, T.; Koritsanszky, T. *XD2016—A Computer Program Package for Multipole Refinement, Topological Analysis of Charge Densities and Evaluation of Intermolecular Energies from Experimental and Theoretical Structure Factors*; University at Buffalo—The State University of New York: New York, NY, USA, 2006.
68. Goddard, T.D.; Huang, C.C.; Meng, E.C.; Pettersen, E.F.; Couch, G.S.; Morris, J.H.; Ferrin, T.E. UCSF ChimeraX: Meeting modern challenges in visualization and analysis. *Protein Sci.* **2018**, *27*, 14–25. [CrossRef]
69. Goddard, T.D.; Kneller, D.G. *SPARKY 3*; University of California: San Francisco, CA, USA, 2008.
70. Altona, C.; Francke, R.; de Haan, R.; Ippel, J.H.; Daalmans, G.J.; Hoekzema, A.J.A.W.; van Wijk, J. Empirical group electronegativities for vicinal NMR proton—Proton couplings along a C-C bond: Solvent effects and reparameterization of the Haasnoot equation. *Magn. Reson. Chem.* **1994**, *32*, 670–678. [CrossRef]
71. Altona, C.; Ippel, J.H.; Hoekzema, A.J.A.W.; Erkelens, C.; Groesbeek, M.; Donders, L.A. Relationship between proton-proton NMR coupling constants and substituent electronegativities. V^{+}—Empirical substituent constants deduced from ethanes and propane. *Magn. Reson. Chem.* **1989**, *27*, 564–576. [CrossRef]
72. Pettersen, E.F.; Goddard, T.D.; Huang, C.C.; Couch, G.S.; Greenblatt, D.M.; Meng, E.C.; Ferrin, T.E. UCSF Chimera—A visualization system for exploratory research and analysis. *J. Comput. Chem.* **2004**, *25*, 1605–1612. [CrossRef]